Polarization-dependent efficient Cherenkov radiation at visible wavelengths in hollow-core photonic crystal fiber cladding*

Shen Xiang-Wei(申向伟)[a)†], Yuan Jin-Hui(苑金辉)[b)], Sang Xin-Zhu(桑新柱)[b)], Yu Chong-Xiu(余重秀)[b)], Rao Lan(饶 岚)[b)], Xia Min(夏 民)[b)], Han Ying(韩 颖)[c)], Xia Chang-Ming(夏长明)[c)], Hou Lan-Tian(侯蓝田)[c)], Wu Zhong-Chao(吴中超)[a)], and He Xiao-Liang(何晓亮)[a)]

[a)] *The 26th Institute of China Electronics Technology Corporation, Chongqing* 400060, *China*

[b)] *State Key Laboratory of Information Photonics and Optical Communications, Beijing University of Posts & Telecommunications, Beijing* 100876, *China*

[c)] *Institute of Infrared Optical Fibers & Sensors, Qinhuangdao* 066004, *China*

(Received 10 June 2012; revised manuscript received 27 June 2012)

Efficient Cherenkov radiation (CR) is experimentally generated by a soliton self-frequency shift (SSFS) in a knot of hollow-core photonic crystal fiber (HC-PCF). When the angle of the half-wave plate is rotated from 0° to 45°, the Raman soliton shifts from 2227 to 2300 nm, the output power of the CR increases 8.15 times, and the maximum output power ratio of the CR at 556 nm to the residual pump is estimated to be 20:1. The width of the output optical spectrum at visible wavelengths broadens from 25 to 45 nm, and the conversion efficiency of the CR can be above 28%. Moreover, the influences of the pump polarization and wavelength on the CR are studied, and the corresponding nonlinear processes are discussed.

Keywords: polarization-dependent Cherenkov radiation, hollow-core photonic crystal fiber (HC-PCF)

PACS: 41.60.Bq, 42.65.Tg, 42.70.Mp, 42.81.Gs **DOI:** 10.1088/1674-1056/22/1/014102

1. Introduction

Photonic crystal fibers (PCFs)[1–9] have opened a new phase for high field physics and nonlinear optics of ultra-short pulses[10–14] due to strong field confinement in the small fiber core, and the possibility of tailoring the dispersion of guided modes by varying the fiber's structure. Cherenkov radiation (CR), known as nonsolitonic radiation or dispersive wave generation, originates from a soliton perturbed by higher order dispersion.[15–17] Cherenkov radiation generation in a photonic crystal fiber (PCF) has attracted great interest due to the remarkable radiation in the visible region.[18–20] Highly efficient CR at the visible wavelength is important for generating a useful laser source for applications such as biophotonics, calibration of astrophysical spectrographs, and ultra-short pulses. Chang *et al.* experimentally demonstrated CR with a pump pulse of 10 fs in PCF, and discussed the influence of the pulse parameters on the bandwidth and the conversion efficiency. However, if the width of the pump pulse is above 100 fs, the conversion efficiency and bandwidth of CR in the visible wavelength will be low and narrow.[17] Yuan *et al.* experimentally achieved CR with a pump pulse of 120 fs, and discussed the influence of the pump power and wavelength on the bandwidth and the conversion efficiency in the fundamental mode of PCF.[21] However, the influences of the higher pump power on the conversion efficiency and the polarization properties of CR in hollow-core photonic crystal fiber (HC-PCF) are not considered. Yan *et al.* experimentally showed the polarization-dependent visible supercontinuum generation in the nanoweb fiber but with a low efficiency.[22]

In this paper, highly efficient CR are generated by soliton self-frequency shift (SSFS) in a knot of HC-PCF. The influences of the pump polarization and wavelength on CR are investigated. When the angle of the half-wave plate rotates, the Raman soliton shifts from 2227 to 2300 nm, the width of the output optical spectrum at the visible wavelength broadens from 25 to 45 nm, and the conversion efficiency of the CR in the experiment can be above 28%. Moreover, the influence of other factors on our experimental process are elementarily analyzed.

2. Properties of HC-PCF and experimental setup

The beam propagation method (BPM)[23] has been used to analyze the properties of group velocity dispersion D of a knot of HC-PCF. Figure 1 shows the group velocity dispersion D, where $D = -(2\pi c)/(\lambda^2)\beta_2$, $\beta_2 = \partial^2\beta(\omega)/\partial\omega^2$, and $\beta(\omega)$ is the fiber mode-propagation constant, calculated as a function of wavelength for the fundamental mode of the knot of HC-PCF with zero dispersion wavelength at 7261 nm. The cross-section structure of HC-PCF is shown in inset 1 of Fig. 1, where the average cladding air hole diameter $d =$ 4.78 μm, hole to hole pitch $\Lambda = 5.69$ μm, and core diameter $d = 20.44$ μm. The zoomed knot of HC-PCF is shown in inset 2 of Fig. 1.

*Project supported by the National Basic Research Program of China (Grant Nos. 2010CB327605 and 2010CB328300), the Fundamental Research Funds for the Central Universities of Ministry of Education of China (Grant Nos. 2011RC0309 and 2011RC008), and the Specialized Research Fund for the Doctoral Program of Beijing University of Posts and Telecommunications, China (Grant No. CX201023).

†Corresponding author. E-mail: xswen_1212@163.com

© 2013 Chinese Physical Society and IOP Publishing Ltd

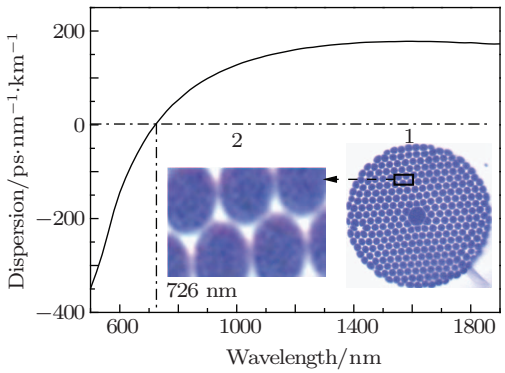


Fig. 1. (color online) Group-velocity dispersion as a function of radiation wavelength for the fundamental mode of the knot of HC-PCF. The vertical dash dot line points to the zero dispersion wavelength of 726 nm. Insets 1 and 2 show the whole and the zoomed knot cross-section of HC-PCF used in the experiment.

The configuration of our experimental setup is given in Fig. 2. The light source is a mode-locked Ti: sapphire laser, emitting a pulse train with full width at half maximum (FWHM) of 120 fs at the repetition rate of 76 MHz. A variable attenuator is placed behind the laser to control the input energy, and an isolator is inserted to block the back-reflection from the input tip of the fiber into the laser cavity. A polarizer is used to purify the input polarization and a rotating half-wave plate is put between the fiber input end and the polarizer to adjust the input polarization. Several 40× objective lenses with numerical aperture of 0.8 are used for adjusting input and output efficiency. CCD1 and CCD2 are used to observe the output mode field and check the coupling state of the input field, respectively. With the offset pumping technique, the fundamental mode can be selectively excited. The beam goes through the first split-beam mirror. One part is coupled to a power meter to monitor the average input power, and the other part is coupled to a 50-cm segment of HC-PCF. The coupling efficiency is above 20%. The transmission loss is 8 dB/m at 820 nm with the cutback method. The output spectra are monitored by two optical spectrum analyzers (OSA, Avaspec-256 and Avaspec-NIR-256) with measurement scopes from 200 to 1100 nm and 900 to 2500 nm, and resolutions of 0.025 and 15 nm.

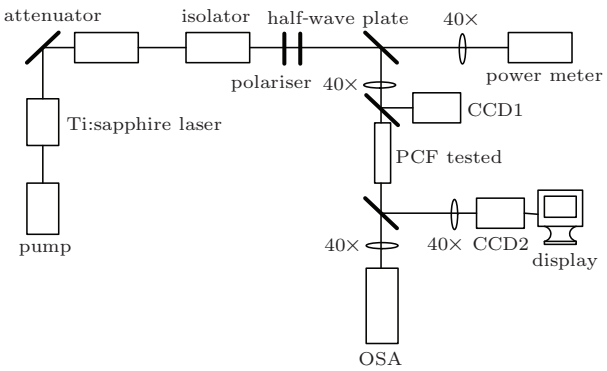


Fig. 2. Configuration of experimental setup.

3. Results and discussion

The experimental conditions and SSFS process are carefully optimized. The experiment is carried out by coupling the fs pulse with a working wavelength from 810 to 830 nm (lying in the anomalous dispersion region), and the average input power is 500 mW into the HC-PCF.

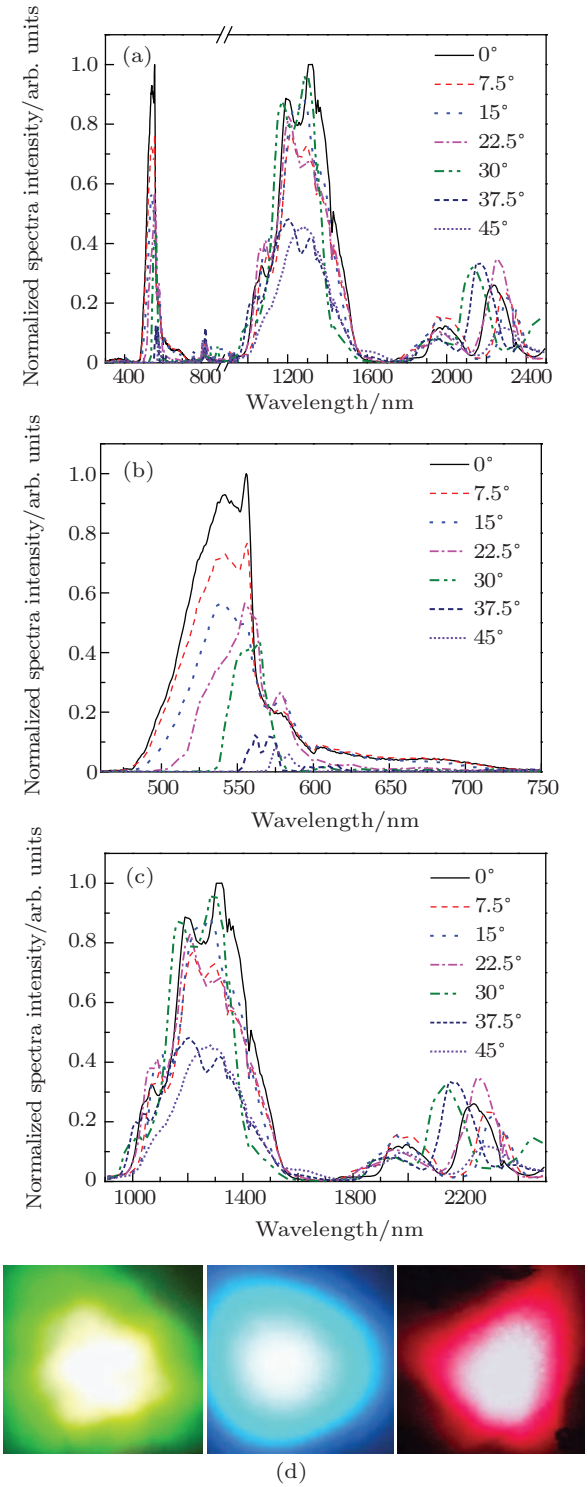


Fig. 3. (color online) (a) The output spectra from 200 to 2500 nm; (b) the zoomed output spectra of CR; (c) the zoomed output spectra from 900 to 2500 nm; (d) the corresponding far field observed at different wavelengths. The pump works at 820 nm and the average input power is 500 mW.

With $\theta = 0°$ and the pump wavelength at 820 nm (θ is the angle between the polarization direction of the mode direction and the input pulse), the output spectra are shown in Fig. 3. By rotating the half-wave plate measuring the output spectra at the fiber end, we can identify the $\theta = 0°$ angle with a maximum output CR.[20] When $\theta = 0°$, the pump power is greatly transferred into the most appropriate mode for the Raman induced SSFS process. Because of the interplay between the SPM and the negative dispersion, the fundamental solitons are formed. Due to the intra-pulse Raman scattering (IRS), this Raman-type amplification appears. Subsequently, when the blue-shift waves and the red-shift solitons are phase matched, the CR and high-order dispersion are generated. During the soliton shift process, the group velocity of solitons continuously decreases, so the XPM traps the CR, resulting in the equal group velocities of the two waves. The pump power is greatly transferred into the CR and the solitons. When the half-wave plate is rotated to $\theta = 7.5°$, some pump power is transferred into another mode, so the power of the most appropriate mode is reduced. The nonlinear optical interaction of the laser becomes weak as the power of the most appropriate mode is reduced, the radiation wavelength increases and the absorption rate of the silica material decreases. As a result, the Raman induced SSFS slows down. When the angle θ of the half-wave plate is rotated from 0° to 45°, the pump power transferred into the Raman soliton shifts from 2227 to 2300 nm, the second soliton is generated from 1193 to 1314 nm, and the SSFS process gradually weakens, as shown in Fig. 3. The corresponding far field observed at different wavelengths is shown in Fig. 3(d).

In Figs. 4(a) and 4(b), when the pump wavelength λ_P is 810 and 830 nm, respectively, the CR is also generated at visible wavelengths by SSFS. With the angle θ of the half-wave plate rotated from 0° to 45°, the output spectra are greatly influenced. In Fig. 4(c), η is the ratio of the output power of CR to the output power of the residual pump, and B is the bandwidth (3 dB) of the CR. On the whole, when θ changes from 0° to 45°, η of the CR slows down, because the power of the most appropriate mode reduces as the half-wave plate is rotated. When λ_P is 820 nm and θ is 0°, η is about 20. When λ_P is 820 and 830 nm, on the whole, B also slows down as θ is increased. This is also due to the previously mentioned reasons. However, when λ_P is 810 nm, as θ changes from 22.5° to 45°, the change in B has a contrary trend (compared to the case where λ_P is 820 and 830 nm), because the peak wavelength shifts from 559 to 632, as shown in Fig. 4(a). When λ_P is 820 nm and θ is, B is up to 45 nm. In this experiment, a conversion efficiency of 28% and B of 45 nm are obtained. The nonlinear process depends on the pulse width, the pump power, fiber structure, λ_P, and suitable polarization. Therefore, a more remarkable CR can be achieved by choosing the optimum conditions.

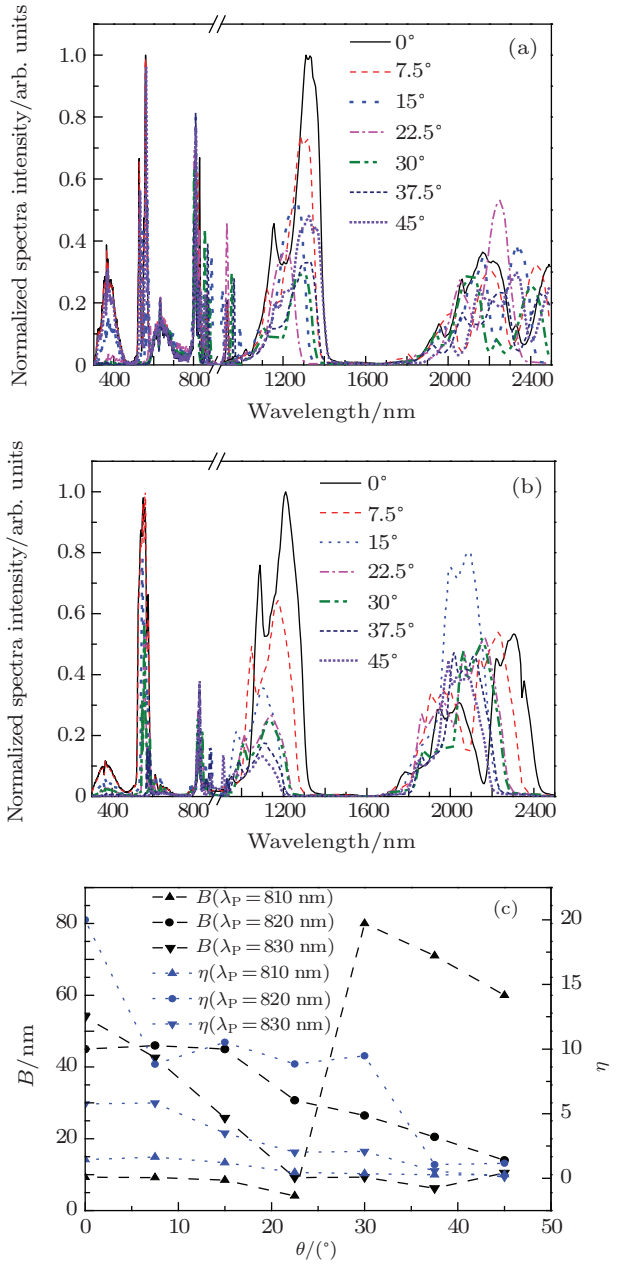


Fig. 4. (color online) (a) Spectra with the pump wavelength λ_P at 810 nm; (b) spectra with the pump wavelength λ_P at 830 nm; (c) bandwidth B (3 dB) and η as functions of θ. The average input power is 500 mW, and the output spectra range from 300 to 2500 nm.

4. Conclusions

In summary, by coupling a train of femtosecond pulses with 120-fs pulse width at a repetition rate of 76 MHz into HC-PCF, highly efficient (28%) and broadband (45 nm) CR is generated. We show that the pump wavelength λ_P and polarization can considerably influence B and η. Moreover, the corresponding nonlinear processes are discussed. These results provide an effective approach to obtaining a signal source at short wavelength.

References

[1] Cregan R F, Mangan B J, Knight J C, Birks T A, Russell P St J, Roberts P J and Allan D C 1999 *Science* **285** 1537

[2] Yuan J H, Sang X Z, Yu C X, Wang K R, Yan B B, Shen X W, Han Y, Zhou G Y, Li S G and Hou L T 2012 *IEEE Photon. Technol. Lett.* **24** 670
[3] Yuan J H, Sang X Z, Yu C X, Li S G, Zhou G Y and Hou L T 2010 *IEEE J. Quantum. Electron*. **46** 728
[4] Shen X W, Yu C X, Sang X Z, Yuan J H, Han Y, Xia C M, Hou L T, Rao L, Xia M and Yin X L 2012 *Acta Phys. Sin*. **61** 044203 (in Chinese)
[5] Shen X W, Yuan J H, Sang X Z, Yu C X, Rao L, Xin X J, Xia M, Han Y, Xia C M and Hou L T 2012 *Chin. Phys.* B **21** 074209
[6] Smith C M, Venkataraman N, Gallagher M T, Muller D, West J A, Borrelli N F, Allan D C and Koch K W 2003 *Nature* **424** 657
[7] Zhao H, Chen M and Li G 2012 *Chin. Phys.* B **21** 068404
[8] Liu S, Li S G, Yin G B and Wang X Y 2012 *Chin. Phys.* B **21** 034217
[9] Han Y, Hou L T, Zhou G Y, Yuan J H, Xia C M, Wang W, Wang C and Hou Z Y 2012 *Chin. Phys. Lett*. **29** 054208
[10] Gorbach A V and Skryabin D V 2008 *Opt. Express* **16** 4858
[11] Hong K H, Hou B, Nees J A, Power E and Mourou G A 2005 *Appl. Phys.* B: *Lasers Opt.* **81** 447
[12] Hauri C P, Kornelis W, Helbing F W, Heinrich A, Couairon A, Mysyrowicz A, Biegert J and Keller U 2004 *Appl. Phys.* B: *Lasers Opt.* **79** 673
[13] Yuan J H, Sang X Z, Yu C X, Xin X J, Li S G, Zhou G Y and Hou L T 2010 *Chin. Phys.* B **19** 074218
[14] Dupriez P, Poletti F, Horak P, Petrovich M N, Jeong Y, Nilsson J, Richardson D J and Payne D N 2007 *Opt. Express* **15** 3729
[15] Wai P K A, Menyuk C R, Lee Y C and Chen H H 1986 *Opt. Lett.* **11** 464
[16] Akhmediev N and Karlsson M 1995 *Phys. Rev.* A **51** 2602
[17] Chang G Q, Chen L J and Krtner 2010 *Opt. Lett.* **35** 2361
[18] Tu H and Bopppart S A 2009 *Opt. Express* **17** 9858
[19] Mitrofanov A V, Linik Y M, Buczynski R, Pysz D, Lorenc D, Bugar I, Ivanov A A, Alfimov M V, Fedotov A B and Zheltikov A M 2006 *Opt. Express* **14** 10645
[20] Hill S, Kuklewicz C E, Leonhardt U and Konig F 2009 *Opt. Express* **17** 13588
[21] Yuan J H, Sang X Z, Yu C X, Han Y, Zhou G Y, Li S G and Hou L T 2011 *IEEE Photon. Technol. Lett*. **23** 786
[22] Yan P G, Shu J, Ruan S C, Zhao J, Zhao J Q, Du C L, Guo C Y, Wei H F and Luo J 2011 *Opt. Express* **19** 4985
[23] Hadley G R 1998 *J. Lightw. Technol.* **46** 34